**Defense Threat Reduction Agency**
**8725 John J. Kingman Road, MS-6201**
**Fort Belvoir, VA 22060-6201**

DTRA-TR-14-58

# TECHNICAL REPORT

# Physics of Radiation Exposure and Characterization for Future Electronic Materials

December 2014

HDTRA1-11-1-0022

Richard M. Osgood, et al.

Prepared by:
The Trustees of Columbia University
615 West 131 Street
Room 254/Mail Code 8725
New York, NY 10027

**DESTRUCTION NOTICE:**

# REPORT DOCUMENTATION PAGE

| 1. REPORT DATE *(DD-MM-YYYY)* | 2. REPORT TYPE | 3. DATES COVERED *(From - To)* |
|---|---|---|

**4. TITLE AND SUBTITLE**

**5a. CONTRACT NUMBER**

**5b. GRANT NUMBER**

**5c. PROGRAM ELEMENT NUMBER**

**6. AUTHOR(S)**

**5d. PROJECT NUMBER**

**5e. TASK NUMBER**

**5f. WORK UNIT NUMBER**

**7. PERFORMING ORGANIZATION NAME(S) AND ADDRESS(ES)**

**8. PERFORMING ORGANIZATION REPORT NUMBER**

**9. SPONSORING / MONITORING AGENCY NAME(S) AND ADDRESS(ES)**

**10. SPONSOR/MONITOR'S ACRONYM(S)**

**11. SPONSOR/MONITOR'S REPORT NUMBER(S)**

**12. DISTRIBUTION / AVAILABILITY STATEMENT**

**13. SUPPLEMENTARY NOTES**

**14. ABSTRACT**

**15. SUBJECT TERMS**

| 16. SECURITY CLASSIFICATION OF: | | | 17. LIMITATION OF ABSTRACT | 18. NUMBER OF PAGES | 19a. NAME OF RESPONSIBLE PERSON |
|---|---|---|---|---|---|
| a. REPORT | b. ABSTRACT | c. THIS PAGE | | | 19b. TELEPHONE NUMBER *(include area code)* |

# CONVERSION TABLE

Conversion Factors for U.S. Customary to metric (SI) units of measurement.

```
    MULTIPLY ──────────────────────►  BY ────────────────────►  TO GET
 TO GET ◄──────────────────────  BY ◄────────────────────  DIVIDE
```

| | | |
|---|---|---|
| angstrom | $1.000\ 000 \times E\ {-}10$ | meters (m) |
| atmosphere (normal) | $1.013\ 25\ \ \times E\ {+}2$ | kilo pascal (kPa) |
| bar | $1.000\ 000 \times E\ {+}2$ | kilo pascal (kPa) |
| barn | $1.000\ 000 \times E\ {-}28$ | $meter^2$ ($m^2$) |
| British thermal unit (thermochemical) | $1.054\ 350 \times E\ {+}3$ | joule (J) |
| calorie (thermochemical) | $4.184\ 000$ | joule (J) |
| cal (thermochemical/$cm^2$) | $4.184\ 000 \times E\ {-}2$ | mega joule/$m^2$ ($MJ/m^2$) |
| curie | $3.700\ 000 \times E\ {+}1$ | *giga bacquerel (GBq) |
| degree (angle) | $1.745\ 329 \times E\ {-}2$ | radian (rad) |
| degree Fahrenheit | $t_k = (t^\circ f + 459.67)/1.8$ | degree kelvin (K) |
| electron volt | $1.602\ 19\ \ \times E\ {-}19$ | joule (J) |
| erg | $1.000\ 000 \times E\ {-}7$ | joule (J) |
| erg/second | $1.000\ 000 \times E\ {-}7$ | watt (W) |
| foot | $3.048\ 000 \times E\ {-}1$ | meter (m) |
| foot-pound-force | $1.355\ 818$ | joule (J) |
| gallon (U.S. liquid) | $3.785\ 412 \times E\ {-}3$ | $meter^3$ ($m^3$) |
| inch | $2.540\ 000 \times E\ {-}2$ | meter (m) |
| jerk | $1.000\ 000 \times E\ {+}9$ | joule (J) |
| joule/kilogram (J/kg) radiation dose absorbed | $1.000\ 000$ | Gray (Gy) |
| kilotons | $4.183$ | terajoules |
| kip (1000 lbf) | $4.448\ 222 \times E\ {+}3$ | newton (N) |
| kip/$inch^2$ (ksi) | $6.894\ 757 \times E\ {+}3$ | kilo pascal (kPa) |
| ktap | $1.000\ 000 \times E\ {+}2$ | newton-second/$m^2$ ($N{-}s/m^2$) |
| micron | $1.000\ 000 \times E\ {-}6$ | meter (m) |
| mil | $2.540\ 000 \times E\ {-}5$ | meter (m) |
| mile (international) | $1.609\ 344 \times E\ {+}3$ | meter (m) |
| ounce | $2.834\ 952 \times E\ {-}2$ | kilogram (kg) |
| pound-force (lbs avoirdupois) | $4.448\ 222$ | newton (N) |
| pound-force inch | $1.129\ 848 \times E\ {-}1$ | newton-meter (N-m) |
| pound-force/inch | $1.751\ 268 \times E\ {+}2$ | newton/meter (N/m) |
| pound-force/$foot^2$ | $4.788\ 026 \times E\ {-}2$ | kilo pascal (kPa) |
| pound-force/$inch^2$ (psi) | $6.894\ 757$ | kilo pascal (kPa) |
| pound-mass (lbm avoirdupois) | $4.535\ 924 \times E\ {-}1$ | kilogram (kg) |
| pound-mass-$foot^2$ (moment of inertia) | $4.214\ 011 \times E\ {-}2$ | kilogram-$meter^2$ ($kg{-}m^2$) |
| pound-mass/$foot^3$ | $1.601\ 846 \times E\ {+}1$ | kilogram-$meter^3$ ($kg/m^3$) |
| rad (radiation dose absorbed) | $1.000\ 000 \times E\ {-}2$ | **Gray (Gy) |
| roentgen | $2.579\ 760 \times E\ {-}4$ | coulomb/kilogram (C/kg) |
| shake | $1.000\ 000 \times E\ {-}8$ | second (s) |
| slug | $1.459\ 390 \times E\ {+}1$ | kilogram (kg) |
| torr (mm Hg, $0^0$ C) | $1.333\ 22\ \ \times E\ {-}1$ | kilo pascal (kPa) |

*The bacquerel (Bq) is the SI unit of radioactivity; 1 Bq = 1 event/s.

**The Gray (GY) is the SI unit of absorbed radiation.

## Abstract

This program achieved fundamental understanding of radiation damage mechanisms in 3 important emerging electronic materials: complex oxides, graphene, and diamond. Our work used advanced materials probes to understand the basic mechanisms of radiation interaction with these three electronic and photonic materials. This work included examination of device- ready (e.g. FETS, optical modulators, spintronics) and thin-film forms. Radiation sources at Brookhaven National Lab., Univ. of Albany, and Pacific Northwest Labs were utilized. The program educated 4 graduate students and yielded many papers and invited talks. Radiation is shown to cause degradation due to displacement and total dose damage.

## The major goals of the project are to:

• Understand radiation interactions, damage mechanisms in advanced and emerging electronic materials.
• Examine the following 3 advanced emerging electronic materials:
  ✓ Graphene
  ✓ Complex metal oxides
  ✓ Diamond
• Develop new radiation-damage characterization techniques that are appropriate for these new material systems

## Accomplishments

### 1) Major Activities

Our program has investigated damage mechanisms in advanced and emerging electronic materials and device structures. Our selection of materials included the advanced materials: graphene, complex metal oxides, and diamond. The program has examined these materials via the following instrumentation: STM, aberration-corrected TEM, ion-beam probing, Raman micro-probing, transport measurement, and optical defect spectroscopy and imaging. The classes of radiation being examined include gamma rays, X-rays, and high-energy beta and alpha particles.

We also have developed the needed materials preparation methods for all three materials, which has included developing the structure and fabrication processes for our test devices and characterizing the unirradiated materials and operational properties. We have carried out a battery of test exposures by α, β and λ particles and performed an analysis on the devices that have been irradiated to determine damage physics and the impact of this damage on device performance.

Our effort also benefits from interactions with Brookhaven National Laboratory, Pacific Northwest National Laboratory, Sincrotronne ELETTRA, Lockheed Martin, NASA, and the State University of New York at Albany (Albany Nanotech). The number of interactions with outside laboratories has increased as the program results have grown.

**2) Specific objectives**

Our objectives listed by material types were as follows:

*Graphene*
Y1. Electrical analysis of defects caused by radiation damage; effect of proton, neutron, alpha, beta, X-ray, electron-beam, and UV sources.
• Development of CVD and delamination-based graphene structures
• Electrical measurements of baseline devices + irradiated devices
• Inverse modeling of FOMs and device parameters
Y2. Characterization of damaged graphene films through scanning probe and TEM techniques–
Use of STM on irradiated samples
• Analysis of samples with HR-TEM
• Modeling of tunneling current spectroscopy and TEM structure for defect identification
Y3. Optical spectroscopy of electronic defect states in graphene systems
• Develop of photocurrent spectroscopy stand for graphene analysis
• Use selective optical excitation together with electrical measurement to analyze nature and behavior of traps caused by different exposures

*Complex Oxides*
Y1: Study of X-ray, $\alpha$, $\beta$, $\gamma$ radiation damage in thin film oxides
• TEM and SEM imaging studies of damage to $LiNbO_3$ and $SrTiO_3$ using $\alpha$ particles
• Preliminary experiments on $LiNbO_3$ and $SrTiO_3$ damage mechanisms using TEM from
$\alpha$, $\gamma$, and $\beta$ and X-ray exposure
Y2: Study of X-ray, $\alpha$, $\beta$, $\gamma$ radiation damage in thin film oxides
• Complete X-ray, $\alpha$, $\gamma$, and $\beta$ damage studies for $LiNbO_3$ and $SrTiO_3$. Assess this damage via an E/O device. Measure $\alpha$-damage mechanisms in other oxides such as $HfO_2$ and $ZrO_2$ samples.
• Investigate short-pulse-initiated carrier dynamics in $LiNbO_3$ and $SrTiO_3$
Y3: Study of X-ray, $\alpha$, $\beta$, $\gamma$ radiation damage in thin film oxides
• Examine other E/O device behavior
• Complete studies in $HfO_2$ and other oxides with energetic X-rays and electrons
• Complete short-pulse measurements to examine carrier dynamics in $SrTiO_3$ both inirradiated and *undamaged* films

*Diamond*
Y1. Study of diamond damage by alpha radiation
• Developed new, clean thin-film sample preparation; characterization by TEM, XRD, fluorescence
• Study of crystal damage using electron spin resonance [new characterization technique]
• Atomic-scale study of radiation damage to proton, neutron, alpha, beta, X-ray, and UV sources.
Y2. Study of diamond heavy-ion ($Fe^+$) irradiation
• Characterization by TEM, XRD, fluorescence
• Development and characterization by electron/nuclear spin resonance
Y3. Precision studies of defect damage in diamond
• Irradiation with sub-10 nm spatial resolution to spatially resolve crystal damage: implantation depth and lateral straggle of ion (N) irradiation and alpha irradiation

• Imaging of irradiation damage using optically detected magnetic resonance with ~ 10 nm spatial resolution

3) **Significant results, including major findings, developments, or conclusions (both positive and negative)**

   **(1)** **Brief Comments on Results**

• Experiments were initiated and completed on examining the effects of alpha radiation on complex oxides, $SrTiO_3$ and $LiNbO_3$. This study, using TEM, micro-Raman, and RBS, showed the importance of displacement damage and interstitial $He^+$ in altering optical properties of the oxide crystal.

• We have shown that ion-induced radiation damage in a $LiNbO_3$-thin-film (10 µm-thick) modulator degrades the device performance in the presence of total charge doses of $\geq 10^{16}$ $cm^{-2}$. The experiments also show that the presence of the $He^+$ stopping region, which determines the degree of overlap between the ion-displacement region and the guided optical mode, plays a major role in determining the degree of degradation in modulation performance. Thus our measurements showed that the higher overlap can lead to an additional ~5.5 dB propagation loss. The irradiation-induced change of crystal-film anisotropy $(n_o - n_e)$ of ~36% was observed for the highest total dose used in the experiments. The relevant device extinction ratio, $V_\square L$, and device insertion loss, as well the damage mechanisms of each of these parameters were also determined. A more extensive account is given in **Section 3) (1)** below. See [*H.-C. Huang, J. I. Dadap, G. Malladi, I. Kymissis, H. Bakhru, R. M. Osgood, Jr., "Helium-ion-induced radiation damage in LiNbO₃ thin-film electro-optic modulators" Submitted, Optics Express*].

• Our work yielded a new method of using scanned microRaman imaging, which has been shown to an effective approach to locating and determining the spatial damage distribution of particle damage in complex oxides. See [*H.-C. Huang, J. I. Dadap, I. P. Herman, H. Bakhru, R. M. Osgood, Jr., "Micro-Raman Spectroscopic Visualization of Lattice Vibration and Strain in He⁺-Implanted Single-Crystal LiNbO₃." Opt. Mater. Express 4, 2, 338-345 (2014)*]. A study of this phenomenon has shown that Raman-mode turn on and turn off can be used to probe displacement damage. It has also shown that relatively low-temperature ~300°C, annealing can remove this damage.

• TEM sectioning of ion-damage complex oxides demonstrated and a thinning method developed.

• The importance of irradiation-induced stress from α-radiation has been clearly shown in ion-irradiated complex oxides. See [*H.-C. Huang, J.I. Dadap, O. Gaathon, I.P.Herman, R.M.Osgood Jr., S.Bakhru, H.Bakhru. A Micro-Raman Spectroscopic Investigation of He⁺-Irradiation Damage in LiNbO₃. Opt. Mater. Exp 3, 126, 2013*]. This stress and stress fields can be visualized and mapped with micro-Raman spectroscopy to show clearly the effects of annealing and ion energy. The resulting stress has a major impact on the optical properties of complex oxide crystal.

• Heavy-ion ($Fe^+$) damage has been realized, measured, and studied in complex oxides ($LiNbO_3$). This work has involved a collaboration with University at Albany and PNNL. Our samples have large displacement damage, throughout the crystal. This is a very different distribution than for light-ion irradiation.

• A battery of analytical methods including in-situ RBS/Channeling (Rutherford Backscattering Spectroscopy), confocal micro-Raman imaging, optical microscopy (OM), scanning electron microscopy (SEM), and atomic force microscopy (AFM) were used to investigate heavy-ion (iron) radiation damage in single-crystal $LiNbO_3$. High (~MeV) and low (~100's keV) iron energies, corresponding to different stopping power mechanisms, were used and their associated damage events observed. It was found that the contribution of electronic stopping from high-energy iron gave rise to a lower critical dose for damage formation than using low-energy irradiation. The use of Raman probing and RBS/C provided complementary damage information and its distribution. Co-irradiation of He+ and Fe+ was performed and micro-Raman edge scans clearly illustrate their cumulative depth-dependent damage behavior. The effects of different dose, post-implantation treatment such as annealing, and the comparison of damage and post-irradiation etching properties between light (He+) and heavy (Fe+) ion irradiation were measured. The effect of co-irradiation using He+ and Fe+ demonstrated the feasibility of patterning on micrometer-scale thin LiNbO3 films. *[H.-C. Huang, J. I. Dadap, G. Malladi, S. Manandhar, R. Sesha R Vemuri, V. Shutthanandan, H. Bakhru, R. M. Osgood, Jr. Comparison of damage and the selective etching behavior by light- and heavy-ion bombardment of single-crystal $LiNbO_3$. Submitted, Appl. Phys. Letters].*

• We developed a new thin-film *diamond* sample preparation method for TEM cross sections that is shown to be superior to conventional techniques using focused ion beam (FIB) milling. The technique employs reactive ion etching (RIE) and results in high-purity membranes that were characterized by TEM, XRD, Raman, fluorescence, and optically detected magnetic resonance studies. These studies confirmed higher quality sections of the RIE samples compared to the conventional FIB-produced samples. See our two publications[*J. Hodges, L. Li, E. Chen, M. Trusheim, S. Allegri, M. Lu, and D. Englund. Ultralong spin coherence time 100 nm diamond membranes. New Journal of Physics, 14, 2012; 27. L. Li, M. Trusheim, O. Gaathon, D. Su, K. Kisslinger, C.-J. Cheng, M. Lu, X. Yao, R. M. Osgood, Jr., D. Englund. Reactive ion etching: Optimized diamond membrane fabrication for transmission electron microscopy. J. Vac. Sci. Technol. B 31, 06FF01, 2013*].

• We employed a new optical characterization technique of diamond quality that relies on electron spin resonance of nitrogen vacancy (NV) color centers present inside the diamond crystal. These NV studies reveal crystal damage and evidence of low concentration of paramagnetic impurities, such as atomic impurities at the level of 100 parts per billion. We have developed this technique to the point that it can easily be applied in a wide-field microscope outfitted with microwave excitation capability. This new spin-based characterization technique is now enabling imaging of lattice damage, e.g., through crystal strain, with sub-100 nm spatial resolution. This is the highest precision technique for imaging crystal strain that is currently available, to our knowledge.

• We completed atomistic-scale studies of radiation damage of diamond to alpha radiation and atomic-scale studies of radiation damage to proton, neutron, beta, X-ray, Iron, Boron, and UV sources.

• We developed techniques for crystal ion slicing of diamond membranes with outstanding crystalline quality and optical clarity. The process enables patterning of an array of 200nm-thick membranes with millimeter-to-micrometer dimensions and exfoliation of the thin films from a single-crystal diamond sample via a parallel fabrication process. The optical properties of the films, which are measured using transmission microscopy, Raman and fluorescence spectroscopy,  showed evidence high quality diamond membranes. For instance, we were able to measure nitrogen-vacancy emission spectra having the zero-phonon line (ZPL) peak of negatively charged centers in an unshifted spectral position suggesting high quality crystalline material. See our publication [*O. Gaathon, J.S. Hodges, E.H. Chen, L. Li, S. Bakhru, H. Bakhru, D. Englund, and R.M. Osgood Jr. Planar fabrication of arrays of ion-exfoliated single-crystal-diamond membranes with nitrogen-vacancy color centers. Optical Materials, 35, 361, 2013*].

• We developed a new technique for ion implantation with extremely small spatial resolution below 10 nm and compatibility with a wide range of target samples. Spatially patterned *ion implantation* plays an important role in numerous fabrication schemes of semiconductor and can also be used to study radiation damage processes. This highly versatile process for ion implantation with high spatial precision  employs a flexible contact mask that can be deposited on a variety of substrates without the need for layer deposition or mask processing on the substrate itself.  The same implantation mask may also be used for pattern transfer via plasma etching in a process that enables precise alignment of implantation and nanostructures simultaneously allowing openings less than 10 nm across and over 250 nm in depth. We have filed for a patent on this work (credited fully to DTRA) and have prepared a manuscript for submission [*I. Bayn, E. H. Chen, L. Li, M. E. Trusheim, T. Schroeder, D. Englund. Nanoscale ion implantation using conformal contact masks.To be submitted in June 2014*].

• Using the ion irradiation and etching techniques developed under DTRA support [*J. Hodges, L. Li, E. Chen, M. Trusheim, S. Allegri, M. Lu, and D. Englund. Long-lived NV− spin coherence in high-purity diamond membranes. New Journal of Physics, 14, 2012.;  L. Li, E. Chen, J. Hodges, M. Lu, O. Gaathon, Jr. R. Osgood, D. Englund. Reactive ion etching: optimized diamond thin-membrane fabrication for transmission electron microscopy. Journal of Vacuum Science and Technology,31 2013.*], we developed a technique for the scalable production of ultra-high-purity diamond nanocrystals. The combination of long spin coherence time and nanoscale size made nitrogen vacancy (NV) centers in nanodiamonds that are critical for quantum information and sensing applications. However, currently available high-pressure high-temperature (HPHT) nanodiamonds have a high concentration of paramagnetic impurities that limit their spin coherence time to less than 1% of that in bulk diamond. In our work, we developed a fabrication process that employs a porous metal mask and a reactive ion etching process to fabricate nanocrystals of high-purity diamond. This work showed that NV centers in these nanodiamonds possess spin coherence times in excess of 200 μs, about two orders of magnitude better than any previous nanocrystals. Since diamond nanocrystals are sensitive to irradiation via the electron spin properties of the NV center, these nanocrystals may be employed as sensitive radiation dosimeters on surfaces or embedded in other materials. See our publication  [*M. E. Trusheim, L.*

*Li, A. Laraoui, E. H. Chen, O. Gaathon, H. Bakhru, C. A. Meriles, D. Englund. Scalable fabrication of high purity diamond nanocrystals with long-spin-coherence nitrogen vacancy centers. Nano Letters 14, 2014*].

• We performed studies of material properties of diamond nanocrystals and nanocrystal surfaces to understand the material properties and radiation effects of high-pressure, high-temperature (HPHT) diamond. Using optical spectroscopy, electron spin resonance, TEM, and Near Edge X-ray Absorption Spectroscopy (NEXAFS), we demonstrated that HPHT diamond nanocrystals have crystallographic and electronic ordering that matches fundamental properties of bulk diamond to the nanoscale while retaining its fluorescing capability. In turn, this class of HPHT ND shared few similarities with detonation nanodiamonds (DNDs). In the process, we were able to discern fundamental differences between HPHT NDs and DNDs. Our observations connected fundamental bulk, surface and color center properties of nanoscale diamond, providing new understanding that impacts their use across disciplines, from quantum computing to microscopy, sensing and biological applications. [*A. Wolcott, T. Schiros, M. E. Trusheim, E. H. Chen, D. Nordlund, R. E. Diaz, O. Gaathon, D. Englund, J. S. Owen. The best of both worlds: Bulk diamond properties realized at the nanoscale. Submitted, ACS*].

• CVD growth of high-quality single-layer graphene was demonstrated using a copper foil catalyst and a newly developed large-grain high pressure CVD process. The material used was fabricated in a furnace installed and facilitated by our group, and the performance of these devices is competitive with exfoliated graphene devices.

• Large-area lithographically processed graphene test devices were demonstrated using CVD graphene films and a new, transfer/release process that reduces any surface residue present on the graphene devices after the transfer process. The properties of these films were characterized via Raman scattering and electron-transport. *[K. Alexandrou, N. Petrone, J. Hone, I. Kymissis. Encapsulated Graphene FETs for air stable operation. Submitted, Nano Letters]*.

• Measurements of the Raman analysis of the graphene film has demonstrated the high quality of the films. Raman analysis has also been applied to these exceptionally low baseline signal samples after radiation exposure to analyze the mechanism of damage.

• Damage in graphene devices has been analyzed using FTIR analysis to determine the exact mechanism of damage in devices and identify the change in bonding associated with graphene device damage.

• It has been demonstrated using testing in sealed bombs that a reaction with water vapor in air causes much of the low-dose TID damage in graphene, whereas higher dose damage is caused by fixed charge in underlying substrate. This insight was used to develop a radiation-hardened GFET incorporating a vapor barrier which was validated using Co-60 gamma irradiation under 260kRad dose exposure. *[K. Alexandrou, J. F. Wishart, N. Petrone, J. Hone, I. Kymissis. Radiation hardened Graphene Field Effect transistors. Submitted, Nano Letters]*.

• Air vapor encapsulation was demonstrated to have virtually no effect on heavy ion/displacement damage

• Electrical and optical testing of the graphene devices has been developed, and a dedicated test bench was established for testing and analysis.

• An encapsulation strategy for ambient operation of high performance CVD graphene was demonstrated and validated. Stable performance of state-of-the-art graphene in air has been demonstrated over a time period longer than two months.[*K. Alexandrou, J. Hone, I.. Kymissis. Encapsulated Graphene FETs for air stable operation. Submitted, Nano Letters*].

• An *in-situ* microcontroller-based measurement system has been built and validated, which automatically measures the performance of graphene devices (I-V characteristics, mobility, and Dirac point) during radiation exposure. This system was used for atmospheric exposure and used to test graphene devices during an in-space exposure on Lambda-Sat, which is a satellite being launched on a Cubesat platform from the International Space Station in June 2014.

• A platform for graded gamma irradiation has been established and graphene devices on a variety of substrates are being analyzed using this platform.

• Our DTRA effort sponsored a successful seminar series during our 3 contract years.

• Our effort also benefited from interactions with Brookhaven National Laboratory, Pacific Northwest National Laboratory, Sincrotronne ELETTRA, Lockheed Martin, NASA, and the State University of New York at Albany (Albany Nanotech). The number of interactions with outside laboratories increased as the program results grew.

## (2) More Extensive Discussion of Selected Results

### a) Complex Oxides

Complex oxides, especially those having perovskite or perovskite-like structures, exhibit remarkable physical properties and a wide variety of functionalities. These oxides, as well their epitaxial thin films, have been well-demonstrated for the use in advanced microdevices such as high-performance acoustic and photonic applications. **Figure 1(a)** shows an example of such
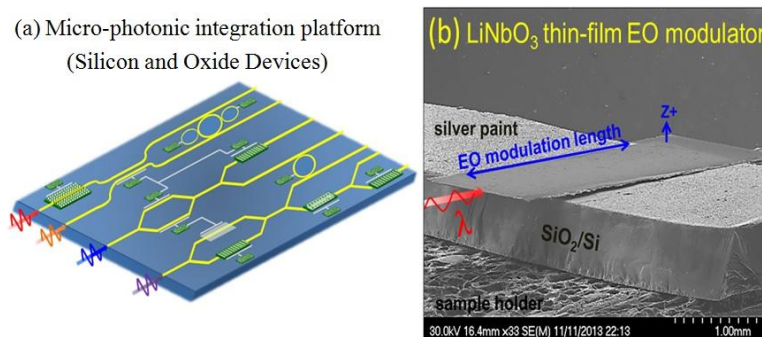


**Fig. 1.** (a) Micro-photonic integration platform for future microelectronics and high data-rate optical communications. (b) unirradiated $LiNbO_3$ thin-film (~10μm) electro-optic modulator.

platform for future micro-photonic integration and high data-rate optical communication systems. Our choice of a key oxide device for examining radiation effects is a LiNbO$_3$ thin film modulator. Oxide devices are expected to be integrated with CMOS circuitry for detection and driving to examine radiation effects. With regard to this perspective, LiNbO$_3$ thin-film electro-optic modulator (~10 µm) has been fabricated using crystal ion slicing and its radiation tolerance has also been carried out. For an unirradiated device, an 8 − 10 dB extinction ratio, V$_\pi$L ~ 7.5 V-cm with ~2 dB insertion loss are measured. Figure 1(b) is an SEM image showing the prototype unirradiated device. LiNbO$_3$ thin-film electro-optic modulator (~10 µm) was effects fabricated using crystal ion slicing. For an unirradiated device, an 8 − 10 dB extinction ratio, V$_\pi$L ~ 7.5 V-cm with ~2 dB insertion loss were measured. **Figure 1(b)** is an SEM image showing the prototype unirradiated device.
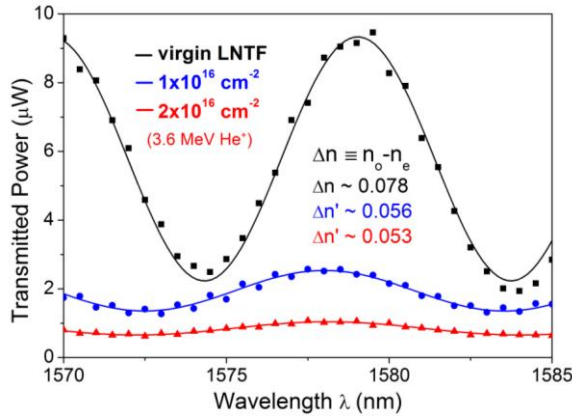


**Fig. 2.** Measured data showing that as the dose is increased, device performance degrades, viz a ~9 dB additional waveguide loss, ~5 dB lower extinction ratio and a ~73% increased V$_\pi$L value indicating degradation for a dose of $2\times10^{16}$ cm$^{-2}$.

After ~$10^{16}$ cm$^{-2}$ He$^+$ bombardment, the irradiation gives rise to a strained thin film. In addition, after a He$^+$ dose of $5\times10^{16}$ cm$^{-2}$, in some cases, thin film partially cracks. Irradiation results in the formation of point and extended defects and the induced long-range strain inside the modualtor. Such radiation damage gives rise to significant light Rayleigh scattering from defects and crystalline damage (loss of material birefringence). The device performance is more downgraded as the irradiation dose is increased. For example, a He$^+$-$2\times10^{16}$ cm$^{-1}$-dose irradiation led to an additional waveguide loss of ~9 dB, a ~5 dB lower extinction ratio, and a ~73% degraded V$_\pi$L value for the modulator. **Figure 2** shows the measured data.

**Table 1** summarizes the device parameters in the presence of different irradiation conditions and examples of the corresponding damage mechanisms.

b) Radiation Damage in Graphene Transistors

| Thin Film (~10 µm thick) | Prototype | 2.3 MeV | 3.6 MeV He$^+$ dose (cm$^{-2}$) | | | Damage Mechanism |
|---|---|---|---|---|---|---|
| | | $1\times10^{16}$ | $1\times10^{16}$ | $2\times10^{16}$ | $5\times10^{16}$ | |
| Extinction Ratio (dB) | ~8 – 10 | ~6.5 dB lowered | ~4 dB lowered | ~5 dB lowered | ~6.2 dB lowered | 1. Lattice disorder (strain) 2. Light scattering from interstitials |
| V$_\pi$L (V-cm) | ~7.5 | ~9.5 (~27%↑) | ~10 (~33%↑) | ~13 (~73%↑) | N.A.* | 1. Lattice disorder 2. Electrodes damage |
| Insertion Loss (dB) | ~2 | ~13 | ~7.5 | ~11.3 | ~16 | 1. Absorption 2. Damage at interface 3. Light scattering |

**\*Films are partially cracked**

**Table 1.** Summary of the device parameters in the presence of different irradiation conditions and examples of the corresponding damage mechanisms. It is clear that as the dose is increased, the damage is greater. Note that 2.3 MeV He$^+$ stops in the center of the film, resulting in higher overlap of the damage with the guided mode. This high overlap leads to lower extinction ratio and higher insertion loss, compared with damage from 3.6 MeV He$^+$ under the same dose.

Our first goal was to develop a high yield and quality transfer - fabrication process for grapheme field effect transistors. After growing a high quality single layer film of carbon on top of 25um copper foils via Chemical Vapor Deposition (CVD) we had to carefully transfer it to our target substrate ($Si/SiO_2$) in order to continue with our transistor fabrication. Raman spectroscopy was conducted after the transfer in order to verify that the graphene was both single layer and defect free (absence or small D-peak in Raman spectra) and with minimal chemical doping; see **Fig.3**.
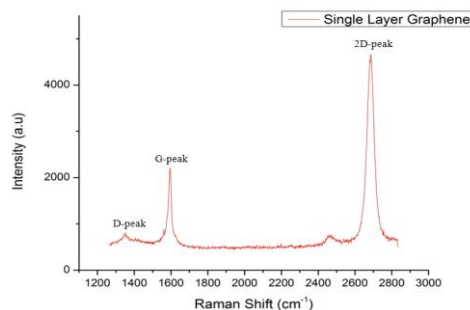


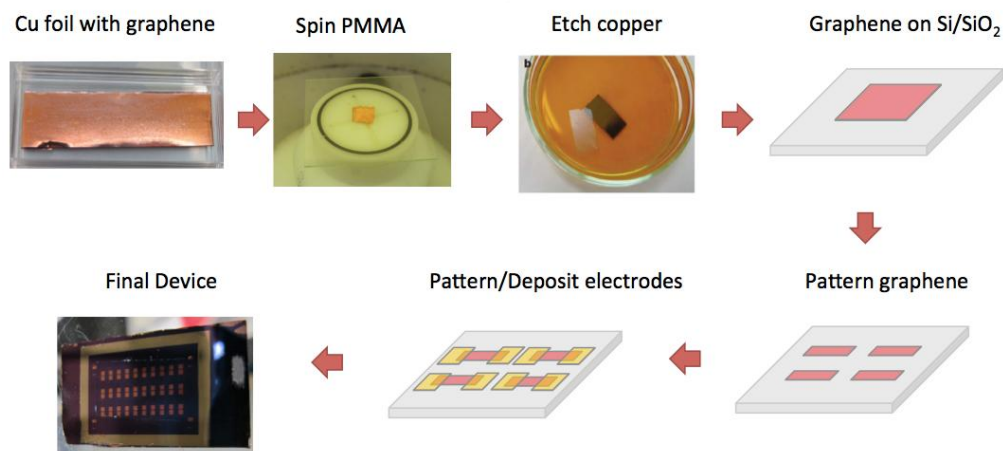**Fig. 3**. Raman spectrum of CVD graphene.



**Fig. 4.** Synthesis and transfer of monolayer graphene from copper foils.

Chemical doping during the transfer process played a significant role in the electronic performance of graphene FETs, as it can limit mobility and shift the Dirac point away from the ideal 0V value. We developed a dry-wet transfer method that in addition of the PMMA spin on top of graphene, incorporated PDMS stamps, in order to let the graphene-PMMA-PDMS stack dry further and eliminate water that otherwise would be trapped between the graphene – $SiO_2$ interface acting as a p-dopant; see **Fig.4**.
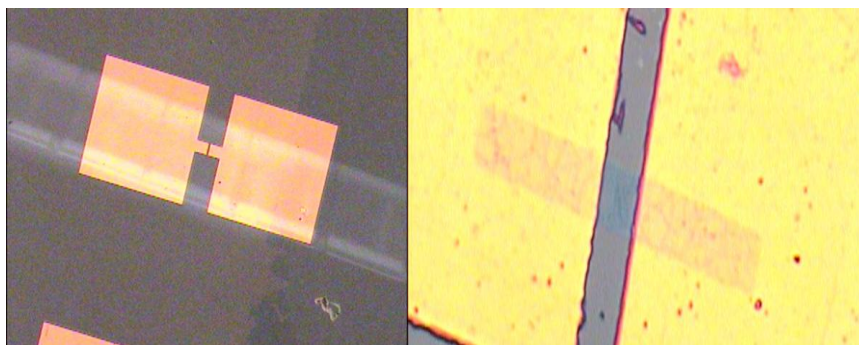
After successfully transferring the graphene film onto the $Si/SiO_2$ substrate, a



**Fig. 5.** Graphene FETs made at Columbia University.

10

series of lithographic steps were conducted in order to pattern the drain and source electrodes (Cr/Au contacts) for the fabrication of various size (W/L) devices. Below in **Fig.5.** are some examples of GFETs with a W/L of 10um patterned on the final substrate.

Electrical characterization of the devices was conducted showing good performing devices with mobilities up to 1250 cm$^2$/Vs and Dirac point very close to zero (5V-10V) indicating high quality transfer and fabrication method. All measurements were conducted at room temperature and in ambient atmosphere environment without any further thermal of current annealing.

- Encapsulation of GFETs for air stable operation

Our first fabricated devices were bottom-gate FETs with the graphene channel exposed to air without any additional top layer in order to protect or encapsulate the graphene. This led to performance degradation through time (days to weeks period) as graphene was exposed to air (with oxygen and water considered major p-dopants) and instability in the electrical behavior of the transistors; see **Fig.6**. In order to solve the stability and doping problem of our devices we developed an encapsulation method that gave us stable and consistent electrical performance for months, with no degradation or doping problems. This was an important step before starting the radiation exposures, since any device instability before or after the radiation would limit our ability to draw safe conclusions.
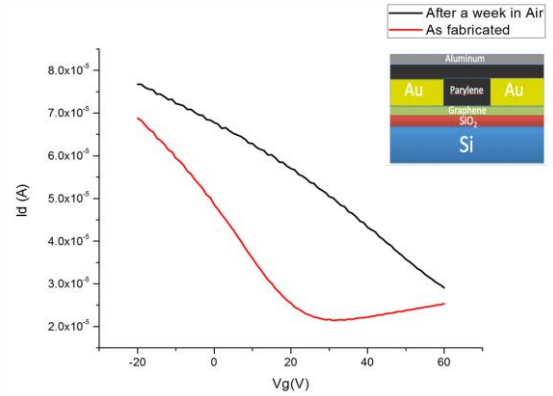


**Fig. 6.** Degradation of a graphene FET in air (black)

Deposition of 1um of Parylene-C and 50nm of thermally evaporated aluminum on top of the graphene channel resulted in the formation of a water and oxygen barrier ensuring the air stability of our transistors; see **Fig.7.**

- Radiation Exposure

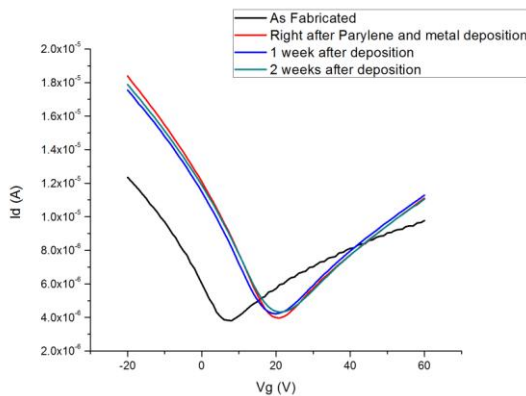Radiation exposures were conducted in collaboration with Brookhaven National Laboratories



**Fig. 7.** Use of Parylene-covered metal to encapsulate a graphene transistor.
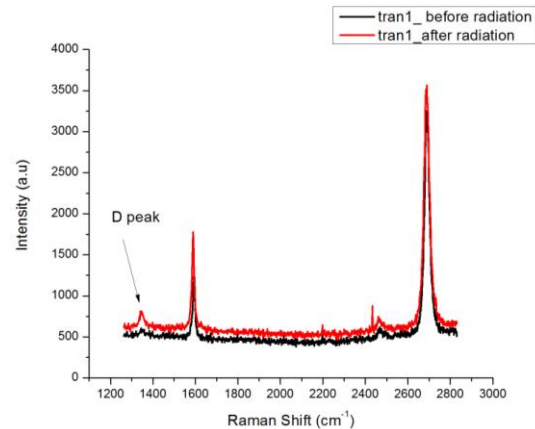


**Fig. 8.** Growth of a D-peak in the Raman spectra feature in graphene due to irradiation

(Dept of Chemistry) and Pacific Northwest National Laboratory (PNNL). We tested our devices under a variety of radiation sources (E-beam, Gamma rays, Fe+ Ions) and energies as pre and post exposure analysis was conducted in order to verify the effects of radiation on graphene devices.

First we found a clear indication that exposure to 3.2Mrad Gamma rays (Co-60 source) can induce a large D-Peak in the graphene lattice; see **Fig.8.** Second, our initial experiments showed, 260Krad of Gamma on nonencapsulated devices clearly affects electronic performance.

However, no performance degradation was found for an encapsulated device using the same 260Krad of gamma rays exposure.
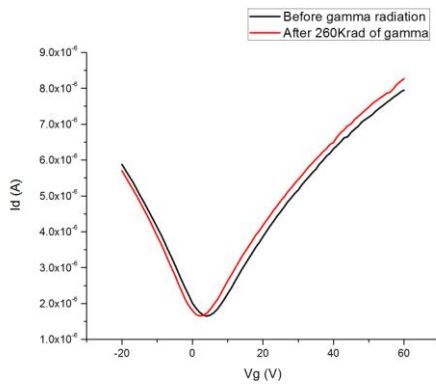


**Fig. 9.** Data showing that encapsulation does protect a graphene device during Gamma exposure.



We also showed, using a 1.5MeV E-beam irradiation, that for nonencapsulated devices that increasing radiation dose degrades device.
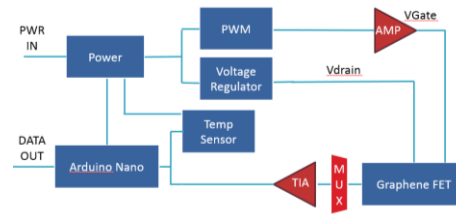
**Fig. 10.** Board block diagram and the actual circuit board for space irradiation testing of graphene devices.

- *In-situ* microcontroller based measurement system.

We designed and built an microcontroller based measurement system for *in-situ* measurements of graphene devices; see **Fig.10**. This system can measure the performance (I-V characteristic, mobility, Dirac point) of the devices before and after exposure and send us the results for further analysis. That circuit board was integrated in the L-sat mission, which is a joint cubesat project across Columbia University, San Jose State University and NASA Ames research center. The project started since March 2013 towards a June 2014 launch with Orbital Sciences Orb-2 ISS resupply mission to the International Space Station. L-sat will give us the opportunity to test these devices in a real space environment.

c) Reactive Ion Etching: optimized diamond membrane fabrication for transmission electron microscopy

To investigate crystal damage in diamond at an atomistic level, the Englund group first developed a new technique to produce high-purity samples for transmission electron microscopy (TEM). We had first produced TEM samples using the typical way, which employ slicing of thin

membranes using a focused ion beam (FIB). However, we found that this method produces low-quality crystals which made the irradiation studies by TEM impossible for moderate irradiation doses. Therefore, we developed a technique to produce thin membranes of diamond by patterning of a bulk crystal with 50-200 nm thick mask lines, and subsequent reactive ion etching (RIE). The RIE process with oxygen gas produced far cleaner diamond surfaces and bulk diamond properties *[L. Li, M. Trusheim , O. Gaathon , K. Kisslinger , C.-J. Cheng , M. Lu , D. Su , X. Yao , H.-C. Huang , I. Bayn , A. Wolcott , R. M. Osgood, Jr. , D. Englund Reactive ion etching: optimized diamond membrane fabrication for transmission electron microscopy. Journal of Vacuum Science and Technology B, Vol. 36, 2013].* We believe that the process is also applicable to many other materials as a replacement for FIB-based sample preparation.
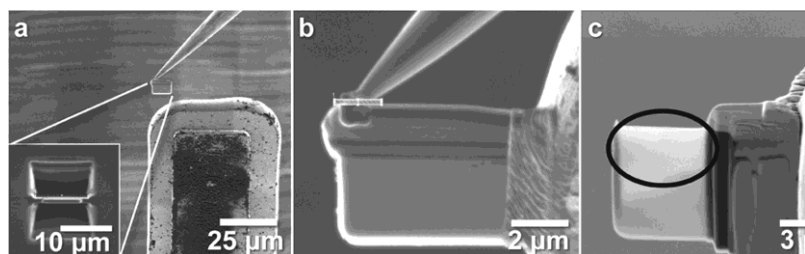


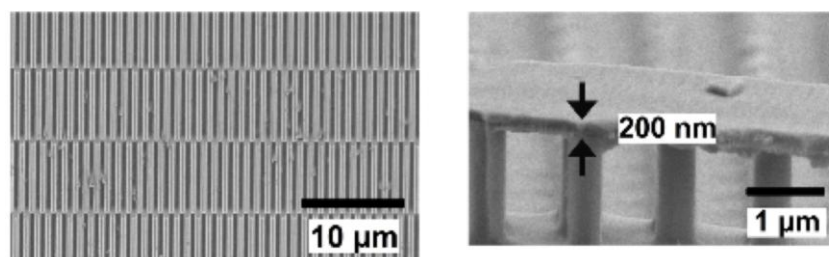**Fig. 11.** TEM cross sectional samples produced using FIB.



**Fig.12.** TEM cross sectional membrane produced by reactive ion etching. Left: Top view of patterned membranes in a bulk single crystal diamond. Right: membranes mechanically removed from the parent crystal and transferred onto silicon spacer posts.
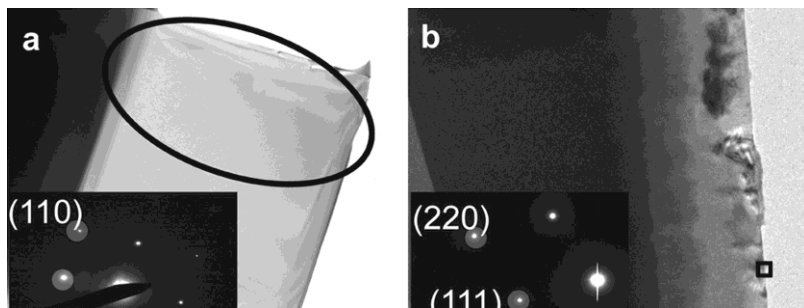


**Fig. 13**. Left: Graphitization region for TEM samples prepared by the typical FIB process:  SRIM simulation indicate Ga implantation at ~14nm. Right: No graphitization in RIE-produced diamond TEM samples.

To compare the RIE and FIB methods, we produced cross-sectional membranes in single crystal diamond using both methods. Figure DirkFig1 shows a membrane produced using FIB; **Fig. 12** shows membranes produced using RIE. The samples were examined by Raman spectroscopy and high-resolution transmission electron microscopy (TEM). The Raman spectra indicated that the crystalline structure of the RIE-processed diamond is preserved, while the FIB-processed diamond membrane has a broad-background sp2 feature. Atomic-resolution TEM imaging (**Fig. 13**) demonstrates that the RIE-based process produces no detectable damage, while the FIB-processed sample has an amorphous carbon layer of about 11 nm thick. These findings show that the RIE-based process allows the production of diamond TEM samples with

reduced near-surface damage and can thus enable direct examination of growth defects and crystallographic damage induced by processes such as ion implantation and bombardment. More

broadly, our study emphasizes the importance of minimally invasive techniques to generate TEM samples for TEM studies with atomic resolution.
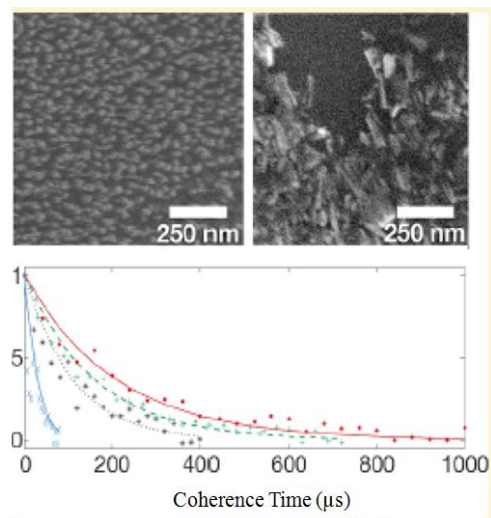


**Fig. 14.** Top left: diamond nanopillars produced by RIE. Top right: diamond nanopillars after mechanical removal and transferring onto new substrate. Bottom: Optically detected magnetic resonance (ODMR) results from nitrogen vacancy (NV) color centers in diamond nanocrystals show record-long spin-coherence times in excess of 200 us.

Our high-purity process of fabricating diamond nanostructures enabled us to produce diamond nanocrystals with record long spin coherence times in nitrogen vacancy (NV) color centers. NV centers have attracted wide interested because of their combination of long spin coherence, which make it an excellent probe for precision sensing applications. However, currently available high-pressure high-temperature (HPHT) nanodiamonds have a high concentration of paramagnetic impurities that limit their spin coherence time to the order of microseconds, less than 1% of that observed in bulk diamond. We employed a self-assembled metal mask to pattern diamond nanorods from high-purity chemical vapor deposition (CVD) diamond, as shown in Fig. DirkFig4. We showed that NV centers in these CVD nanodiamonds exhibit record-long spin coherence times in excess of 200 μs, enabling magnetic field sensitivies of 290 nT Hz−1/2 with the spatial resolution characteristic of a 50 nm diameter probe *[M. E. Trusheim, L. Li, A. Laraoui, E. H. Chen, O. Gaathon, H. Bakhru, T. Schröder, C. A. Meriles, D. Englund. Scalable Fabrication of High Purity Diamond Nanocrystals with Long-Spin-Coherence Nitrogen Vacancy Centers. Nano Letters 14, 2013].* This advance will enable precision magnetic field sensing with a spatial resolution on the order of 10 nm. The ability to image magnetic fields with such precision brings nuclear magnetic resonance imaging to the nanometer scale and could represent an important tool for studying radiation damage at the atomistic level. This work was highlighted in a Nature News Feature *[http://www.nature.com/news/quantum-physics-flawed-to-perfection-1.14565].*

### 4) Key Outcomes or Other Achievements

• A new method of using scanned microRaman imaging has been shown to an effective approach to locating and determining the spatial damage distribution of particle damage in complex oxides. See [*H.-C.Huang, J.I.Dadap, O.Gaathon, I.P.Herman, R.M.Osgood Jr., S.Bakhru, H.Bakhru. A Micro-Raman Spectroscopic Investigation of He$^+$-Irradiation Damage in LiNbO$_3$. Opt. Mater. Exp 3, 126, 2013*]. A study of this phenomenon is now completed.

• Heavy-ion (Fe+) damage has been realized, measured and studied in complex oxides (LiNbO$_3$).

• The importance of visualization Raman microscopy for examined irradiation induced stress has been clearly shown in ion-irradiated complex oxides. See [*H.-C. Huang, J. I. Dadap, I. P. Herman, H. Bakhru, R. M. Osgood, Jr., "Micro-Raman Spectroscopic Visualization of Lattice*

*Vibration and Strain in He⁺- Implanted Single-Crystal LiNbO₃." Opt. Mater. Express 4, 2, 338-345, 2014*].

• A new method of preparing ultra-high-purity thin film diamond samples for damage experiments has been developed. The high-purity diamond samples were evaluated by TEM, optical Raman, and optically detected magnetic resonance of nitrogen vacancy (NV) centers. The spin coherence time of the NV center was found to be > of 100 microsec, a world record for nanofabricated diamond.

• We have employed a new optical characterization technique of diamond quality that relies on electron spin resonance of nitrogen vacancy (NV) color centers present inside the diamond crystal.

• We have developed a new technique for ion implantation with extremely small spatial resolution below 10 nm and compatibility with a wide range of target samples.

• Large-area lithographically processed graphene test devices have been demonstrated using CVD graphene films and a new, transfer/release process that reduces any surface residue present on the graphene devices after the transfer process.

• An *in-situ* microcontroller-based measurement system has been built and validated, which automatically measures the performance of graphene devices (I-V characteristics, mobility, and Dirac point) during radiation exposure.  This system will be used for atmospheric exposure and will also be used to test graphene devices during an in-space exposure on Lambda-Sat, which is a satellite being launched on a Cubesat platform from the International Space Station in November 2013.

## Training

We worked in a one-on-one mode to train our 5 graduate students and we also trained undergraduate and masters students in specific areas of device fabrication, material science, and electrical device analysis.
Our students and postdocs have participated in many conferences and the annual DTRA workshops.

## Professional development

• Prof. Osgood was an invited participant in a workshop at Brookhaven National Lab to determine the possibility of a suite of new X-ray probes for examining radiation damage in solid materials in 2012. As a result of this workshop it was decided to submit a proposal for a major new beamline at NSLS II, a new billion-dollar synchrotron facility being built on Long Island. The facility is motivated in part by our input on the needs for *in situ* X-ray probes to investigate damage in advanced electronics facility. We have continued our contact with this program and the overall proposal for the beamline has now been accepted. This facility will provide a major facility for radiation testing of materials in the US.  Graduate Student Stan Huang was invited to

attended an additional workshop on this beamline and we have maintained in close technical consultation.

• Our group at Columbia has developed a forum to discuss specific aspects of problems and to present ideas and to provide coordination on the research with one formal meeting per month.

• In visits to Brookhaven National Laboratory, Prof. Englund developed his collaboration on damage by electron and alpha irradiation of diamond using a TEM probe. These visits have included an invited talk at the Annual User's Meeting at BNL in which the DTRA project was highlighted.

• Columbia graduate students. Hsu-Cheng Huang and Peter Bullen were trained in the use of ion implantations at SUNY Albany and ion implantation of heavy elements at PNNL.

• Columbia graduate student Luozhou Li was trained by BNL researchers Dr. Ming Lu on nanofabrication techniques related to the fabrication of ultra-thin diamond membranes that will be used for cross-sectional studies of radiation damage.

• Columbia graduate students Matt Trusheim and Jacob Mower were trained by BNL researcher Kim Kisslinger on diamond membrane fabrication and TEM cross-section sample fabrication.

• Columbia University student Kostas Alexandrou was trained in graphene synthesis by several Columbia students in the Kim, Hone, and Kymissis groups that have experience in graphene, and the optical and electrical analysis of devices by students in the Kymissis and Shepard groups.

• Columbia student Kostas Alexandrou worked on developing a new set of protocols for space qualification and space-radiation hardness testing suitable for the Cubesat program together with staff from NASA and Lockheed-Martin.

• Columbia student Kostas Alexandrou and Prof. Kymissis were trained in electron beam and gamma irradiation, calibration, and dose analysis procedures at Brookhaven National Lab.

• The interactions, visits, and stays at National Lab facilities such as at BNL, PNNL, and NASA provided a major tool for increasing the professional training of our DTRA students.

• Our group at Columbia worked together in a collaborative mode. There have been frequent and important interactions among the PIs and the graduate students in terms of materials science, use of irradiation sources, and device concepts and methodology in our work on the DTRA program. This interaction has formed a tight and productive group.

## Dissemination to Communities of Interest

• We have participated in several professional meetings and conferences, such as the CAARI and APS meeting, an IEEE CMPT workshop, MRS, SPIE, and given talks at these meetings. Our interactions with BNL, PNNL, and Albany are examples of our outreach activities.

• We have initiated a DTRA outreach seminar to develop a dialogue with other members of the DTRA community; our speakers have included, for example, T.P. Ma (Yale), Robert Reed (Vanderbilt), and Corey Cress (NRL). Several follow-on discussions/collaborations and proposals have followed this interaction.

## Plan During Next Reporting Period to Accomplish Goals

This is a final report.

## DEPARTMENT OF DEFENSE

DEFENSE THREAT REDUCTION
AGENCY
8725 JOHN J. KINGMAN ROAD
STOP 6201
FORT BELVOIR, VA 22060
     ATTN: A. LYALIKOV

DEFENSE THREAT REDUCTION
AGENCY
8725 JOHN J. KINGMAN ROAD
STOP 6201
FORT BELVOIR, VA 22060
     ATTN: G. DOYLE

DEFENSE TECHNICAL
INFORMATION CENTER
8725 JOHN J. KINGMAN ROAD,
SUITE 0944
FT. BELVOIR, VA  22060-6201
     ATTN: DTIC/OCA

## DEPARTMENT OF DEFENSE CONTRACTORS

QUANTERION SOLUTIONS, INC.
1680 TEXAS STREET, SE
KIRTLAND AFB, NM  87117-5669
     ATTN: DTRIAC